Journal of Bioenergetics and Biomembranes, Vol. 32, No. 5, 2000

Vanadyl as a Probe of the Function of the F_1-ATPase-Mg^{2+} Cofactor

Wayne D. Frasch[1]

The Mg^{2+} dependent asymmetry of the F_1-ATPase catalytic sites leads to the differences in affinity for nucleotides and is an essential component of the binding-change mechanism. Changes in metal ligands during the catalytic cycle responsible for this asymmetry were characterized by vanadyl $(V^{IV} = O)^{2+}$, a functional surrogate for Mg^{2+}. The ^{51}V-hyperfine parameters derived from EPR spectra of VO^{2+} bound to specific sites on F_1 provide a direct probe of the metal ligands. Site-directed mutations of metal ligand residues cause measurable changes in the ^{51}V-hyperfine parameters of the bound VO^{2+}, thereby providing a means to identification. Initial binding of the metal–nucleotide to the low-affinity catalytic site conformation results in metal coordination by hydroxyl groups from the P-loop threonine and catch-loop threonine. Upon conversion to the high-affinity conformation, carboxyl groups from the Walker homology B aspartate and $MF_1\beta$E197 become ligands in lieu of the hydroxyl groups.

KEY WORDS: F_1-ATPase; F_1F_o-ATP synthase; vanadyl.

The F_1F_oATP synthase uses the nonequilibrium transmembrane gradient derived from photosynthetic light energy or the oxidation of metabolites to drive the reaction $ADP + P_i \leftrightarrow ATP + H_2O$ beyond the point of equilibrium and thereby maintain high cellular concentrations of ATP. Many enzymes use ATP hydrolysis to return the ATP/ADP–P_i chemical gradient toward equilibrium as an energy source for catalysis. Under some conditions, the enzyme can catalyze ATP hydrolysis that pumps protons in the reverse direction across the membrane. However, the F_1F_o from mitochondria and chloroplasts employ specific mechanisms to minimize this reverse reaction.

The intrinsic membrane F_o protein complex mediates proton translocation. The extrinsic membrane F_1 protein complex can be solubilized from the membrane where, in the absence of F_o it can catalyze ATP hydrolysis. Partial structures of soluble F_1 have been determined from bovine mitochondrial F_1, shown in Fig. 1 (Abrahams *et al.*, 1994), rat liver mitochondria (Bianchet *et al.*, 1998), the thermophilic Bacillus *PS3* (Shirakira *et al.*, 1997), *E. coli* (Hausrath *et al.*, 1999), and the F_1F_o from yeast (Stock *et al.*, 1999). The three α and three β subunits, which fold in a similar manner, are arranged alternately like segments of an orange around a large portion of the γ subunit. The binding sites for the nucleotides are at the interfaces between α and β subunits. The catalytic sites are predominantly in the β subunits with some contributions from groups on the α subunits and, conversely, with the noncatalytic sites.

In the structure of F_1 from bovine mitochondria, the three catalytic sites are asymmetric in that one contains bound Mg^{2+}–ADP (β_{DP}), one contains bound Mg^{2+}-AMP–PNP (an analog of ATP) (β_{TP}), and one is empty (β_E) (Abrahams *et al.*, 1994). Such asymmetry was predicted from experiments that served as the basis of the binding-change hypothesis (O'Neal and Boyer, 1984). In this hypothesis, the enzyme adopts a conformation at one of the three catalytic sites in which ADP and phosphate are tightly bound. In this high-affinity conformation, the equilibrium of the $ADP + P_i \leftrightarrow ATP + H_2O$ reaction is close to unity and, therefore, the synthesis of ATP is not the energy-requiring step. Instead, input of energy from the proton gradient is used to drive a conformational change that promotes the release of newly synthesized

[1] Center for the Study of Early Events in Photosynthesis, Department of Plant Biology, Arizona State University, Tempe, Arizona 85287-1601. e-mail: frasch@asu.edu

0145-479X/00/1000-0539$18.00/0

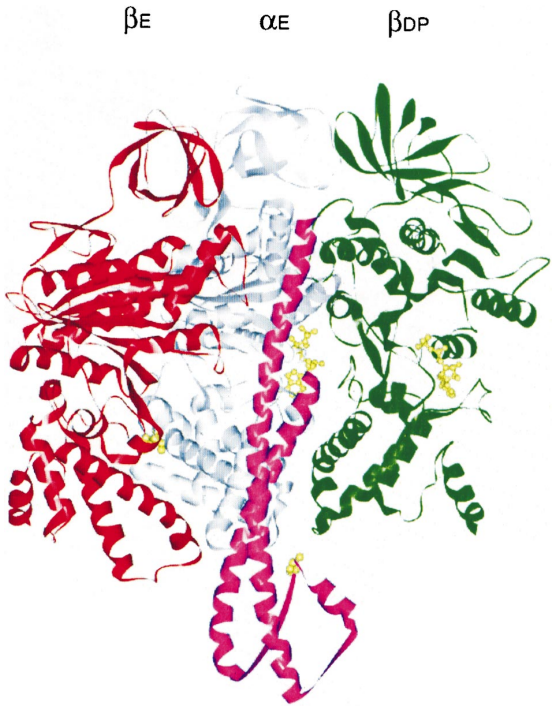

Fig. 1. Cross section of the 2.8 Å crystal structure of F_1 from bovine heart mitochondria (Abrahams *et al.*, 1994) that shows the asymmetry between the empty (β_E) and Mg^{2+}–ADP-containing (β_{DP}) catalytic sites.

ATP. Because this conformational change can only occur when an adjacent empty catalytic site fills with substrate, the conformation of catalytic sites was thought to be staggered and work in a cooperative manner.

The observation that ATPase activity of soluble F_1 drives the rotation of the γ subunit provided insight to questions concerning how the catalytic subunits act in a cooperative manner (Duncan *et al.*, 1995; Sabbert *et al.*, 1996; Noji *et al.*, 1997). The enzyme is, in fact, a molecular motor. In the most compelling demonstration of γ rotation, an actin filament decorated with fluorescent groups was attached to the γ subunit of F_1. Counterclockwise rotation of the actin, driven by ATP hydrolysis, was observed with a fluorescence microscope (Noji *et al.*, 1997). Based on the direction of γ rotation, the sequence of conformations of each catalytic site is $\beta_E \rightarrow \beta_{TP} \rightarrow \beta_{DP} \rightarrow \beta_E$ during ATP hydrolysis.

The asymmetry of the catalytic sites that is necessary for the binding-change mechanism depends on the γ subunit and Mg^{2+}. In the absence of the γ subunit and Mg^{2+}, the crystal structure of the $\alpha_3\beta_3$ complex from the thermophilic Bacillus *PS3* has threefold symmetry (Shirakira *et al.*, 1997). In the rat liver F_1 structure, which was crystallized in the absence of Mg^{2+}, the $\alpha_3\beta_3$ portion of the structure shows threefold symmetry despite the presence of the γ subunit (Bianchet *et al.*, 1998).

The Mg^{2+} induced asymmetry of the catalytic sites is also responsible for the differences in nucleotide affinity between these sites. Using the βY331W mutant in *E. coli* F_1, Weber *et al.* (1993) monitored the catalytic site occupancy from the quenching of the tryptophan fluorescence that occurs when nucleotide is bound. In the absence of Mg^{2+}, the three catalytic sites bind ATP with the same affinity (Weber *et al.*, 1993). However, when ATP binds as a complex with Mg^{2+}, the affinity for nucleotides can differ by as much as five orders of magnitude. This suggests that changes in the ligand environment of Mg^{2+} may be responsible for the observed differences in nucleotide affinity among the catalytic sites.

Magnesium is difficult to study because of the lack of spectroscopic probes. It is also difficult to identify in a protein crystal structure because it has a similar size and electron density to water. We have found vanadyl $(V^{IV}{=}O)^{2+}$ to be a valuable tool to characterize the environment of the Mg^{2+}-binding sites in the F_1-ATPase. Vanadyl has four equatorial ligands and one axial ligand that is *trans* to the oxo group. As a result, the VO^{2+} ligands adopt an octahedral configuration like that of Mg^{2+}. Due to the nuclear spin $I = 7/2$ and the anisotropy of the molecule, the single unpaired electron of VO^{2+} gives rise to an EPR signal that consists of two sets of eight transitions from the fractions of molecules where the V = O bond is aligned parallel and perpendicular to the magnetic field (Fig. 2). The center of each group of eight transitions and the spacing between them is determined by the values of g and A, respectively. The magnitude of these values depends on the strength of the hyperfine coupling between the unpaired electron and the ^{51}V nucleus.

The ^{51}V-hyperfine coupling of VO^{2+} is sensitive to the types of groups coordinated at the equatorial positions (Chasteen, 1981). Figure 2 shows the EPR spectra and hyperfine coupling of VO^{2+} when the four equatorial ligands are either water or hydroxyl groups. The dependence of the position of the $-5/2_{\|}$ transition of the EPR signal on the type of groups ligated is also shown in the inset of Fig. 2. Each ligand contributes independently to the ^{51}V-hyperfine coupling, enabling the complement of the four different ligands to be discerned (Chasteen, 1981; Markham, 1984). Based on the measured coupling constants of $A_{\|}$ from studies of model complexes, the hyperfine coupling for a given group of equatorial ligands can be calculated from the equation

$$A_{\|\text{calc}} = \sum n_i A_{\|i}/4 \qquad (1)$$

where i counts the different types of equatorial ligand donor groups, n_i ($n_i = 1$–4) is the number of ligands of

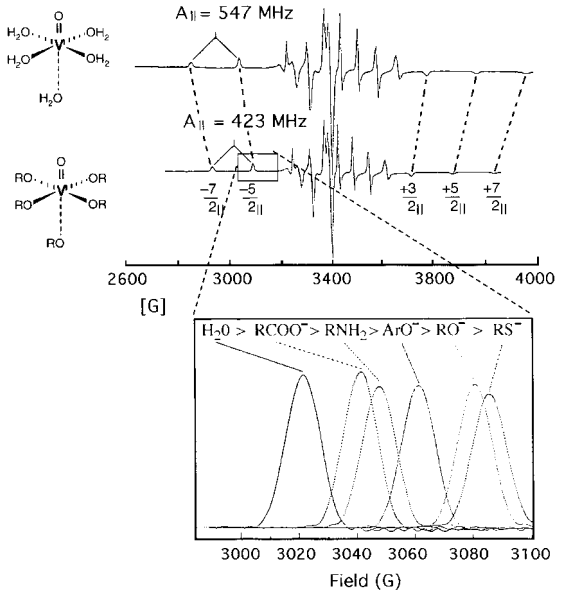

Fig. 2. Equatorial ligands determine ^{51}V-hyperfine, Parameters of VO^{2+}. EPR spectra of VO^{2+} with water (top) or hydroxyl groups (bottom) as equatorial ligands. The parallel transitions ($-7/2_{\|}$, $-5/2_{\|}$, $+3/2_{\|}$, $+5/2_{\|}$, and $+7/2_{\|}$) that are not superimposed with perpendicular transitions are identified. Inset: dependence of the $-5/2_{\|}$ transition on the type of equatorial ligands.

type *i*, and $A_{\|}$ is the measured coupling constant for the equatorial ligand donor group of type *i* (Chasteen, 1981). Similar equations can be written for $g_{\|}$ and for A_{iso}, although the changes in $A_{\|}$ are the largest and most easily discerned. There are 211 possible sets of equatorial ligands to protein-bound VO^{2+} not including the smaller differences due to oxygen coordination by carboxyl groups like aspartate, carbonyl from groups like asparagine, and phosphate, and when rarely occurring groups that result from post-translational modification are excluded.

The intensity of the EPR signal from VO^{2+} free in frozen solution is suppressed by aggregation in HEPES buffer relative to that bound to the protein (Chasteen, 1981). Furthermore, the signal intensity that remains from the unbound VO^{2+} in solution can be distinguished from that which arises from enzyme-bound VO^{2+} when examined at room temperature. At this temperature, the enzyme-bound VO^{2+} species will still resolve the parallel and perpendicular features usually observed at liquid nitrogen temperatures. However, at room temperature, the VO^{2+} in solution will only show the rotationally averaged EPR signal.

Purified spinach chloroplast F_1-ATPase can use VO^{2+} as a functional cofactor for ATP hydrolysis (Houseman *et al.*, 1994a). At metal concentrations equal to or less than that of ATP, higher rates of ATPase activity were observed with VO^{2+} than with either Mg^{2+} or Ca^{2+}. In a manner similar to the free-metal inhibition caused by Mg^{2+}, lower rates of ATPase activity are observed when the VO^{2+} concentration exceeds that of ATP. The rates of VO^{2+} dependent photophosphorylation catalyzed by CF_1F_o in thylakoids are also comparable to those observed with Mg^{2+} as a cofactor, which indicates that VO^{2+} is a functional surrogate for Mg^{2+} in the intact enzyme.

Some studies suggested that some of the six total metal-binding sites known to exist on F_1 were regulatory sites that did not complex with nucleotide (Schobert, 1993). Although the crystal structure confirmed the presence of six metal-binding sites, each was found to be coordinated to the bound nucleotides, and no additional regulatory metal-binding sites were observed (Abrahams *et al.*, 1994). Specific catalytic or noncatalytic binding sites of CF_1 can be depleted and selectively filled with metal-nucleotide complexes (Bruist and Hammes, 1981; Shapiro *et al.*, 1991). Three nucleotide-binding sites were initially characterized that were designated sites 1–3 in order of decreasing affinity for nucleotide. The dissociation constants for ATP or ADP binding to catalytic site 3 are in the micromolar range and can be removed from CF_1 via gel-filtration chromatography. Site 2 binds Mg^{2+}-ATP specifically and with very high affinity. This noncatalytic site remains occupied even after extensive turnover of the enzyme. Depletion of Mg^{2+}-ATP from site 2 requires partial unfolding of CF_1 by precipitation in ammonium sulfate in the presence of EDTA. Gel-filtration chromatography of the resuspended protein with buffer that contains EDTA removes the metal nucleotide from this site. Site 1 is catalytic and contains Mg^{2+}-ADP, which remains bound to the enzyme after extensive dialysis or gel filtration. However, ADP or ATP in the medium will exchange with the nucleotide bound at this site. Subsequently, an additional catalytic site was identified as site 4. This site binds nucleotide extremely tightly like site 1, but can be distinguished from site 1 in that only site 1 can bind TNP–nucleotides (Soteropoulos *et al.*, 1994). Depletion of sites 1 and 4 of metal–nucleotide complex is facilitated by removal of the ε subunit of CF_1 (Xiao and McCarty, 1989).

The catalytic activity of chloroplast F_1 purified from F_o and the thylakoid membrane is latent, although ATPase activity can be activated via reduction of a disulfide bond on the γ subunit (cf Frasch, 1994). The oxidation state of this disulfide provides one of multiple levels of interrelated regulatory mechanisms to minimize ATPase activity of CF_1F_o in thylakoids in the absence of a proton gradient. The dark decay of ATPase activity in thylakoids is accelerated by the addition of ADP that becomes tightly bound in the latent state (Smith and Boyer, 1976). Inhibition of

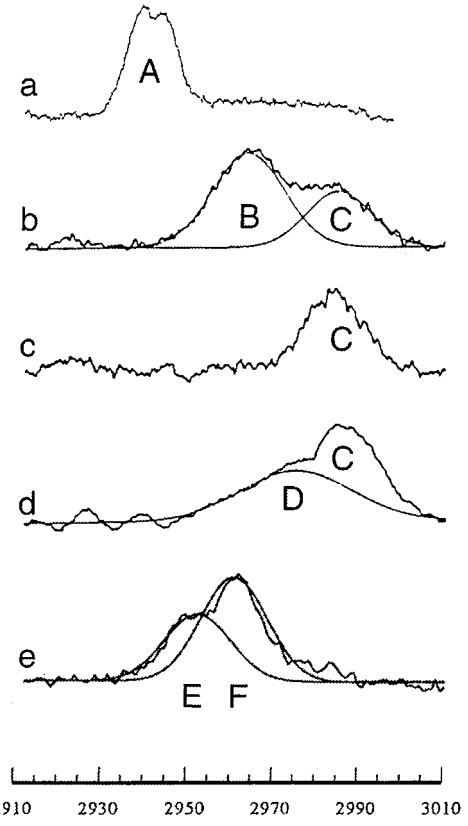

Fig. 3. The $-5/2_{\|}$ transition(s) of VO^{2+} bound to CF_1 as: (a) VO^{2+}–ATP at latent site 2, (b) VO^{2+}–ADP bound to latent site 3, (c) VO^{2+}–ADP bound to activated site 3, (d) VO^{2+}–ATP bound to activated site 3; and (e) VO^{2+}–ATP bound to site 1 using CF_1-ε.

ATPase activity and the increase in affinity of the site for ADP only occur upon the addition of Mg^{2+} (Feldman and Boyer, 1985; Zhou *et al.*, 1988). Under these conditions, the bound ADP apparently forms a complex with Mg^{2+} that prevents further catalysis. This entrapment of Mg^{2+}-ADP serves a regulatory function in F_1-ATPases from other organisms as well (Jault and Allison, 1993, 1994).

Figure 3a shows the $-5/2_{\|}$ transition of VO^{2+} bound as the VO^{2+}–ATP complex to noncatalytic site 2 of latent CF_1 (Houseman *et al.*, 1994, 1995). This EPR signal designated species A was identified as the VO^{2+}–ATP complex at site 2, because this species was not depleted by extensive gel filtration, but required precipitation of the protein in ammonium sulfate and EDTA to remove the metal–nucleotide from this site. The integrated intensity of species A calibrated by atomic absorption spectroscopy of vanadium showed that this species saturated upon binding of about one VO^{2+} per CF_1. Species A exists as a 5.2 G doublet that results from superhyperfine coupling of a ^{31}P nucleus from a single phosphate coordinated at an equatorial position.

Figure 3b shows the $-5/2_{\|}$ line of the EPR spectrum after the addition of one equivalent of VO^{2+}–ADP to latent CF_1 depleted of metal-nucleotide from catalytic site 3 (Houseman *et al.*, 1994, 1995). The binding of VO^{2+}–ADP to site 3 gave rise to two EPR species designated B and C, with the species B form predominant. Activation of ATPase activity of this sample with dithiothreitol caused the signal intensity of species B to convert to species C (Fig. 3c) Although ^{31}P splittings are not well defined in species C, line-shape analyses suggest that this species is comprised of a 1:2:1 triplet characteristic of a bidentate VO^{2+}-ADP complex. The conversion of species B to C upon activation indicates that EPR spectra of bound VO^{2+} can reveal structural changes in the metal-binding site of the enzyme in solution. It is noteworthy that these experiments were carried out at pH 8, which is the pH of the stroma when transmembrane proton gradient maintained by light-driven electron transfer reactions has reached steady state and the F_1F_o is activated buy thioredoxin-mediated reduction of the γ subunit disulfide. In the dark, the stroma reverts to about pH 7 upon collapse of the proton gradient when the enzyme reverts to the latent form. At this pH, the VO^{2+}-nucleotide bound to site three of latent CF_1 is almost exclusively in the form of EPR species B.

When VO^{2+}-ATP is bound to site 3 of latent CF_1, EPR species B and C are also observed in the same proportion as observed in Fig. 3b (Houseman *et al.*, 1995). Upon activation, the signal intensity from species B is converted into species C and an additional species designated D (Fig. 3d). The transitions in species D are significantly broader than observed in the other EPR species. This may be the result of coordination by as many as all three phosphates, although the splitting due to ^{31}P-superhyperfine coupling is not resolved in the spectrum. The metal–nucleotides bound to high-affinity site 1 is more easily depleted from CF_1 after the ε subunit has been removed (Xiao and McCarty, 1989). Addition of an equivalent of VO^{2+}-nucleotide to CF_1-ε results in the formation of EPR species designated E and F (Fig. 3e).

Site-directed mutations of the P-loop threonine, a known metal ligand in bovine MF_1 (Abrahams *et al.*, 1994), were made to the β subunit of *Chlamydomonas* CF_1 to determine if perceptible changes in the EPR spectrum of VO^{2+} bound to catalytic site 3 could be observed (Chen *et al.*, 1999). Each of the three mutations examined was found to alter the ^{51}V-hyperfine tensors of the bound VO^{2+} (Fig. 4). These changes were specific for the VO^{2+}–nucleotide bound in the active conformation of site 3 (EPR species C). In the latent, catalytically inactive

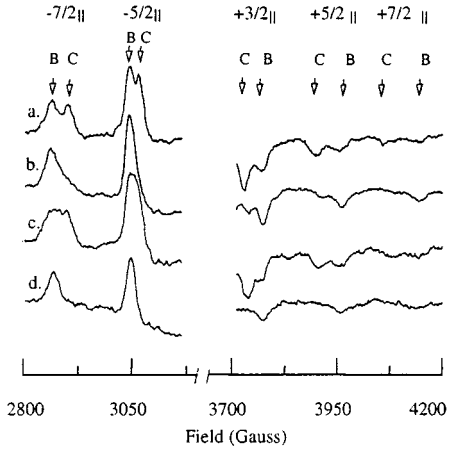

Fig. 4. Changes in the EPR spectrum from VO^{2+}–ATP bound to site 3 of latent *Chlamydomonas* CF_1 as the result of site-directed mutations of $CF_1\beta$T168 (Chen *et al.*, 1999). The parallel transitions of the EPR spectrum that do not overlap with perpendicular transitions are shown for wild-type (a), T68D (b), T168C (c), T168L (d). The transitions that result from EPR species B and C are indicated.

conformation that results in EPR species B, the P-loop threonine mutants did not alter the EPR spectrum of VO^{2+}–nucleotide complex bound to site 3. These data indicated that this technique could be used to identify specific groups as metal ligands. It also demonstrated that the latent form of CF_1 did not have the P-loop threonine as a ligand but that the activation process caused the insertion of this hydroxyl group into the coordination sphere to make the functional form of the enzyme.

Site-directed mutations of the catch loop tyrosine ($MF_1\beta$Y311, $CF_1\beta$Y317 in *Chlamydomonas*) also changed the values of $A_{\|}$ and $g_{\|}$ from EPR species C, but had little effect on those of species B when VO^{2+}–nucleotide was bound to site 3. These data indicate that this residue was also a metal ligand in the activated, but not the latent, conformation of catalytic site 3. Thus, the activated form of site 3, the catalytic site with lowest affinity for the metal–nucleotide complex contains two hydroxyl groups as ligands to the metal cofactor.

Three carboxyl groups, $MF_1\beta$E188, $MF_1\beta$E192, and $MF_1\beta$D256, are within about 5 Å of the Mg^{2+} bound at the catalytic sites in bovine MF_1 such that they can be considered candidates as metal ligands (Abrahams *et al.*, 1994). In this structure, the former carboxyl is hydrogen bonded to a water molecule that is 4.4 Å from the γ-phosphate in β_{TP} of bovine MF_1 (Abrahams *et al.*, 1994), such that this residue could alternatively activate the water to promote nucleophilic attack of the terminal phosphate. The latter carboxyl is in the Walker homology B (WHB) motif that is conserved among several Mg^{2+}–nucleotide-binding proteins (58). The WHB-aspartate has been suggested to hydrogen bond to a water molecule that is coordinated to the metal, or to coordinate to Mg^{2+} directly (Al-Shawi *et al.*, 1992; Yohda *et al.*, 1988; Weber *et al.*, 1998).

None of the mutants to the carboxyl residues analogous to $MF_1\beta$E188, $MF_1\beta$E192, and $MF_1\beta$D256 in the *Chlamydomonas* CF_1 significantly changed the ^{51}V-hyperfine coupling of EPR species C, the activated form of VO^{2+}-nucleotide bound to site 3 (Hu *et al.*, 1996, 1999; Chen *et al.*, 2000). The ^{51}V-hyperfine parameters of EPR species B, the latent form of site 3, were affected only by mutations made to the WHB-aspartate (Hu *et al.*, 1999). Thus, the WHB aspartate is a ligand in the latent form of site 3, but is displaced by the hydroxyl groups as ligands upon activation. The other carboxyl residues are not equatorial ligands to VO^{2+} in site 3 in either the latent or activated forms.

The same mutants to the *Chlamydomonas* CF_1 residues analogous to $MF_1\beta$E192, and $MF_1\beta$D256 were examined for their effects on VO^{2+}–ADP bound to site 1 of CF_1-ε (Chen *et al.*, 2000). Depletion of the ϵ subunit activates the enzyme and facilitates higher occupancy of site 1 with metal–nucleotide complex. The changes in EPR species E and F from catalytic site 1 that result from these mutants indicated that both carboxyl residues are metal ligands to the metal–nucleotide bound at this site.

In the chloroplast enzyme, the catalytic site with highest affinity (CF_1 site 4) binds the metal–nucleotide so tightly that it is difficult to study. The analogous site in *E. coli* F_1 (EF_1, site 1) is much more easily loaded with metal–nucleotide (Weber *et al.*, 1993). The EPR spectrum of VO^{2+} bound as VO^{2+}–ADP to EF_1 is closely similar to EPR species D observed with CF_1 (Fig. 3d). The types of equatorial ligands derived from the best fit of the ^{51}V-hyperfine parameters to Eq. (1) suggest the presence of three oxygens from either phosphate or carboxyl (Asp or Glu) and 1 oxygen from a hydroxyl (Ser or Thr).

The analysis of each mutant by EPR spectroscopy of the VO^{2+} bound to F_1 not only indicates whether the ^{51}V-hyperfine parameters differ from the wild type, but also provides an estimate of the types of groups that the protein used as ligands in its attempt to compensate for the mutation based on Eq. (1). These analyses provide insight into the evolutionary pressures that resulted in the metal ligands used by the F_1. For example, mutation of either a hydroxyl or a carboxyl ligand to a sulfhydryl typically results in the sulfhydryl group as a metal ligand, but will often cause a second ligand to be substituted for a coordinated water.

Mutations of hydroxyl groups for carboxyl groups or the converse tend to cause the greatest disruption to the coordination sphere of the metal bound to the catalytic site. The most likely reason for this is that the enzyme uses

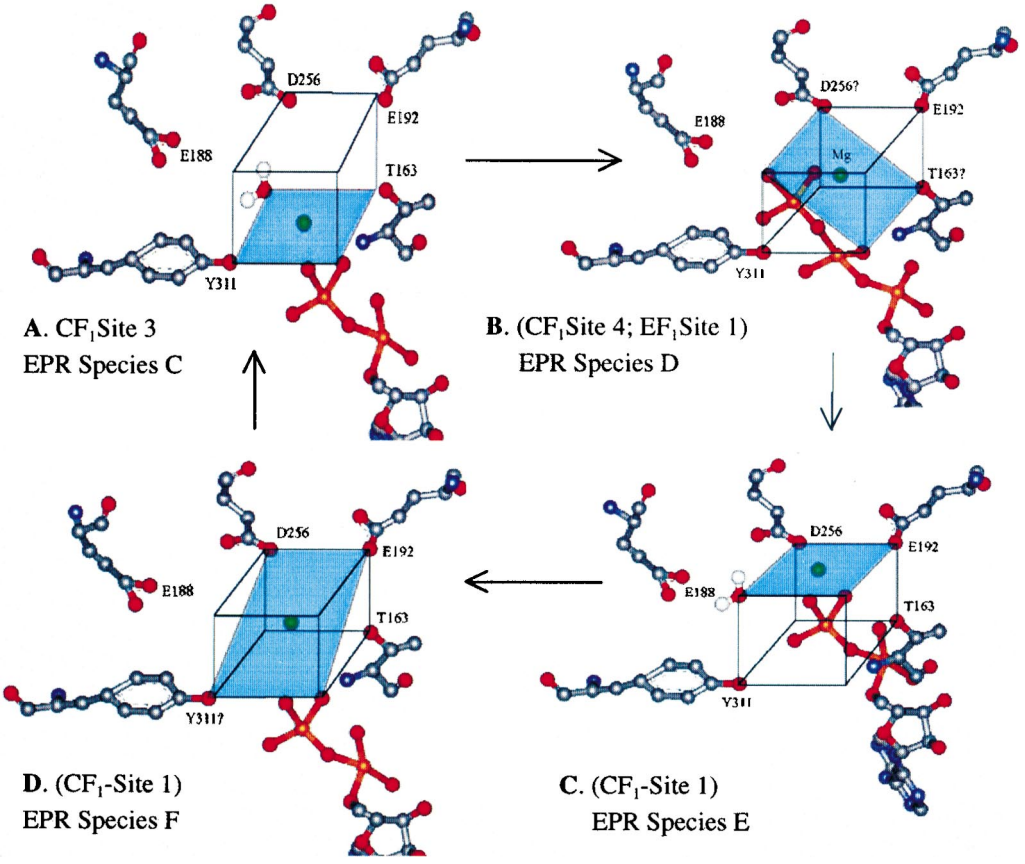

Fig. 5. Changes in metal ligands during the catalytic cycle of F_1-ATPase identified by EPR spectroscopy of VO^{2+}. The equatorial ligands in each conformation are indicated as the residues at the corners of the blue square. The box shown provides an indication of the approximate three-dimensional relationship of the residues. Positive identification of the residues that give rise to EPR species D awaits confirmation with mutagenesis studies.

the hydroxyl and carboxyl ligands in the conformations with low and high affinity for nucleotide, respectively. The conversion between low- and high-affinity conformations appears to be critical to the function of the enzyme.

Figure 5 summarizes the metal ligands identified in the sequential progression of conformational states of each catalytic site during a catalytic cycle of ATPase hydrolysis. The amino acids that serve as ligands in one or more conformations are shown in three-dimensional space approximately as they exist in the catalytic site. These groups roughly define the corners of a cube in the catalytic site. The equatorial ligands to VO^{2+} in each conformation are those residues shown at the corners of the blue square. Side chains indicated with question marks are the best estimate of the ligand in that conformation at this time. In some cases, more work is also required to identify the number of coordinated phosphates.

When the metal–ATP complex initially binds in the low affinity, site 3 conformation, hydroxyl groups from the P-loop threonine and the catch-loop tyrosine form equatorial ligands to VO^{2+} (Fig. 5A). These groups define the bottom plane of the binding pocket. Conversion to the high-affinity (EF_1site 1, CF_1site 4) conformation (Fig. 5B) causes the insertion of a carboxyl group that is likely the Walker B–aspartate ($MF_1\beta$D256) and causes the displacement of the catch-loop tyrosine from the coordination sphere. Upon formation of CF_1 site 1 (Fig. 5C), the metal–nucleotide moves to the top of the binding pocket where the carboxyls analogous to $MF_1\beta$D256 (WHB–aspartate) and $MF_1\beta$193 are equatorial metal ligands. The hydroxyl group (probably the P-loop threonine) is not an equatorial ligand to VO^{2+} in this conformation, but may be an axial metal ligand. In *Chlamydomonas* CF_1 site 1 the VO^{2+}–ADP can exist in two conformation that differ only by one ligand that is either a tyrosine hydroxyl or a water molecule (Fig. 5C and D). If the tyrosine ligand proves to be the catch-loop tyrosine, this form may be an intermediate state between the high-affinity site 1 and the low-affinity site 3 in the final conformational change that completes the catalytic cycle as shown in Fig. 5. Alternatively,

one of the conformations in *Chlamydomonas* CF_1 site 1 may represent the nonfunctional (entrapped) metal–ADP complex thought to regulate the enzyme (Drobinshaya *et al.*, 1985). Recent evidence suggests that this is the site at which the entrapped metal–ADP complex binds (Digel *et al.*, 1998). More experiments are necessary to resolve these possibilities.

In the crystal structure of bovine MF_1 (Abrahams *et al.*, 1994), the helical domain that contains the DELSEED sequence is significantly closer to the P-loop in the catalytic sites that contain Mg^{2+}-nucleotide than is observed in the empty catalytic site. This implies that the helical bundle oscillates up and down during catalysis. Since the Mg^{2+}-nucleotide complex is tethered to the helical bundle via π bonding of the adenine ring with $MF_1\beta$Y345, the upward movement of the helical bundle during the transition of the catalytic site from low to high affinity should also move the metal–nucleotide in the same direction. This movement is consistent with the change in metal ligands from the bottom to the top of the metal-binding pocket shown in Fig. 5. Carboxyl groups coordinate hard metals, such as Mg^{2+}, with higher affinity than do hydroxyl groups. It is noteworthy that the carboxyl and hydroxyl ligands are found in the high- and low-affinity metal–nucleotide conformations, respectively.

The presence of the catch-loop tyrosine as a metal ligand in the low-affinity site may also contribute significantly to the mechanism of ATP synthesis due to its location. In the bovine MF_1 structure (Abrahams *et al.*, 1994), hydrogen bonds between γ subunit residues $MF_1\beta$R254 and γQ255 and β subunit residues $MF_1\beta$D316, $MF_1\beta$T318, and $MF_1\beta$D319 form the "catch" of the catch loop. Under conditions of ATP synthesis, the transmembrane proton gradient will provide a constant torque on the γ subunit. Rotation of this subunit when the catalytic sites are empty would dissipate the proton gradient in a nonproductive manner. However, the energy in the hydrogen bonds between the β and γ subunits, including those at the catch-loop when one of the three catalytic sites is empty, is approximately sufficient to prevent this rotation. When Mg^{2+}–ADP binds to the empty catalytic site, metal coordination by the bulky catch loop tyrosine may deform the catch loop sufficiently to break the hydrogen bonds at this location, thereby triggering γ subunit rotation and conformational changes of all three catalytic sites. Because all three sites change in response to the rotation, one catalytic site will necessarily form the conformation that leads to product dissociation. Hydrogen bonds between the γ subunit and the catch loop of this newly formed empty site would limit the rotation of the γ subunit to 120° per catalytic event and provide an escapement mechanism to insure that proton flux through F_o only occurred when the catalytic sites synthesized ATP.

Vanadyl has been a useful tool to characterize the changes in the ligands of the metal cofactor through the catalytic cycle. As these changes are more completely discerned, the molecular basis for the Mg^{2+} requirement for the catalytic site asymmetry and the associated differences in affinity for nucleotides that enables the enzyme to maintain the chemical gradient of ATP that provides cellular energy are becoming more clear.

ACKNOWLEDGMENT

This work was supported by NIH grant GM-50202.

REFERENCES

Abrahams, J. P., Leslie, A. G. W., Lutter, R., and Walker, J. E. (1994) *Nature (London)* **370**, 621–628.
Al-Shawi, M. K., and Senior, A. E. (1992). *Biochemistry* **31**, 878–885.
Bianchet, M. A., Hullihen, J., Pedersen, P. L., and Amzel, L. M. (1998). *Proc. Natl. Acad. Sci. USA* **95**, 11065–11070.
Bruist, M. F., and Hammes, G. G. (1981). *Biochemistry* **20**, 6298–6305.
Chasteen, N. D. (1981). *In Biological Magnetic Resonance* (Berliner, L. and Reuben, J., eds.), Plenum, New York, pp. 53–119.
Chen, W., Hu, C.-Y., Crampton, D. J., and Frasch, W. D. (2000). *Biochemistry* **39**, 9393–9400.
Chen, W., LoBrutto, R., and Frasch, W. D. (1999). *J. Biol. Chem.* **274**, 7089–7094.
Digel, J. G., Moore, N. D., and McCarty, R. E. (1998). *Biochemistry* **37**, 17209–17215.
Drobinshaya, I. Y., Kozlov, I. A., Murataliev, M. B., and Vulfson, E. N. (1985). *FEBS Lett.* **182**, 419–424.
Duncan, T. M., Bulygin, V. V., Zhou, Y., Hutcheon, M. L., and Cross, R. L. (1995). *Proc. Natl. Acad. Sci. USA* **92**, 10964–10968.
Feldman, R. I., and Boyer, P. D. (1985). *J. Biol. Chem.* **260**, 13088–13094.
Frasch, W. D. (1994). In *The Molecular Biology of Cyanobacteria* (Bryant, D., ed.), Kluwer, The Netherlands, pp. 361–380.
Hausrath, A. C., Gruber, G., Matthews, B. W., and Capaldi, R. A. (1999). *Proc. Natl. Acad. Sci. USA* **96**, 13697.
Houseman, A. L. P., Morgan, L., LoBrutto, R., and Frasch, W. D. (1994a). *Biochemistry* **33**, 4910–4917.
Houseman, A. L., LoBrutto, R., and Frasch, W. D. (1994b). *Biochemistry* **33**, 10000–10006.
Houseman, A. L., LoBrutto, R., and Frasch, W. D. (1995a). *Biochemistry* **34**, 3277–3285.
Houseman, A. L. P., LoBrutto, R., Bell, M., and Frasch, W. D. (1995b). In *Photosynthesis: From Light to Biosphere* (P. Mathis, ed.) Vol. III, Kluwer, The Netherlands, pp. 127–130.
Hu, C.-Y., Houseman, A. L. P., Morgan, L., Webber, A. N., and Frasch, W. D. (1996). *Biochemistry* **35**, 12201–12211.
Hu, C.-Y., Chen, W., and Frasch, W. D. (1999). *J. Biol. Chem.* **274**, 30481–30486.
Jault, J.-M., and Allison, W. S. (1993). *J. Biol. Chem.* **268**, 1558–1566.
Jault, J.-M., and Allison, W. S. (1994). *J. Biol. Chem.* **269**, 319–325.
Markham, G. D. (1984). *Biochemistry* **23**, 470–478.
Noji, H., Yasuda, R., Yoshida, M., and Kinosita, K. (1997). *Nature (London)* **386**, 299–302.
O'Neal, C., and Boyer, P. D. (1984). *J. Biol. Chem.* **259**, 5761–5767.

Sabbert, D., Engelbrecht, S., and Junge, W. (1996). *Nature (London)* **381**, 623–625.
Schobert, B. (1993). *Biochemistry* **32**, 13204–13211.
Shapiro, A. B., Huber, A. H., and McCarty, R. E. (1991). *J. Biol. Chem.* **266**, 4194–4200.
Shirakihara, Y., Kambara, M., Saika, K., Kagawa, Y., and Yoshida, M. (1997). *Structure* **5**, 825–836.
Smith, J. P., and Boyer, P. D. (1976). *Proc. Natl. Acad. Sci. USA* **73**, 4314–4318.
Soteropoulos, P., Ong, A. M., and McCarty, R. E. (1994). *J. Biol. Chem.* **269**, 19810–19816.
Stock, D., Leslie, A. G. W., and Walker, J. E. (1999). *Science* **286**, 1700.
Walker, J. E., Saraste, M., Runswick, M. J., and Gay, N. J. (1982). *EMBO J.* **1**, 945–951.
Weber, J., and Senior, A. E. (1997). *Biochim. Biophys. Acta* **1319**, 19–58.
Weber, J., Wilke-Mounts, S., Lee, R. S.-F., Grell, E., and Senior, A. E. (1993). *J. Biol. Chem.* **268**, 20126–20133.
Weber, J., Hammond, S. T., Wilke-Mounts, S., and Senior, A. E. (1998). *Biochemistry* **37**, 608–614.
Xiao, J., and McCarty, R. E. (1989). *Biochim. Biophys. Acta* **976**, 203–209.
Yohda, M., Ohta, S., Hisabori, T., and Kagawa, Y. (1988). *Biochim Biophys Acta* **933**, 156–164.
Zhou, J. M., Xue, Z., Du, Z., Melese, T., and Boyer, P. D. (1988). *Biochemistry* **27**, 5129–5135.